Materials Science and Engineering B 275 (2022) 115525

Contents lists available at ScienceDirect

Materials Science & Engineering B

journal homepage: www.elsevier.com/locate/mseb

The effect of ultrasonic wave amplitude on the physical properties of zinc oxide (ZnO) deposited by ultrasonic spray method

A. Attaf [a,*], A. Djadai [a], A. Derbali [a], H. Saidi [a], M.S. Aida [b], N. Lehraki [a], N. Attaf [c], R. Attaf [c], L. Derbali [d], M. Poulain [e]

[a] Laboratory of Thin Films and Applications LPCMA, University Mohamed KhiderBiskra, BP 145 RP, 07000 Biskra, Algeria
[b] Department of Physics Faculty of Sciences, King Abdulaziz University, Djeddah, Kingdom of Saudi Arabia
[c] Equipe plasmas et couches minces unité de recherche matériaux et applications, University de Constantine, Algeria
[d] Department of Physics, College of Science and Humanities, Al Quwayiyah, Shaqraa University, Kingdom of Saudi Arabia
[e] Photonic Material Laboratory, University of Rennes, CNRS, IPR (Institute of Physics of Rennes) UMR 6251, F-35000 Rennes, France

ARTICLE INFO

Keywords:
ZnO thin film
Ultrasonic wave amplitude
Physical properties
Spray ultrasonic technique
SEM micrographs

ABSTRACT

In this study, high quality zinc oxide (ZnO) thin films, with improved properties, were prepared by a cost-effective ultrasonic spray pyrolysis technique via a careful optimization of the used ultrasonic wave amplitude. The deposition process was performed on glass substrate and were subsequently annealed at 400 °C. We investigated the effect of various ultrasonic wave amplitude on the structural, surface morphology, optical and electrical properties of the obtained thin films, after varying the applied wave amplitude. Furthermore, deposited thin films were studied by means of XRD, UV–vis spectrophotometer, scanning electron microscope, and four-point probe technique. XRD analysis confirmed that obtained ZnO thin films have polycrystalline structure and a wurtzite (hexagonal) phase, with a c-axis preferred orientation (0 0 2). The crystallite size was about 23–30 nm. The SEM micrographs of the surface morphology show uniform, homogenous and dense films with granular structures. The films thicknesses were found to be dependent on the used wave amplitude; they were ranged from 184 to 423.5 nm. In addition, the optical properties of the deposited thin films reveal that the films are highly transparent in the visible region above 80%, while the value of energy band gap varies from 3.24 to 3.27 eV. The Electrical properties investigation revealed a resistivity around 10^{-3} Ω.cm, showing also a non negligible dependency with the wave amplitude tuning. We obtained an improvement in the carrier concentration (1.6×10^{20}–3.9×10^{20} cm^{-3}) and mobility (4.2–15 cm^2/V.s) with the ultrasonic wave amplitude rising. High quality ZnO thin films with enhanced properties are in demand and have a large wide of applications in optoelectronics and solar cells.

1. Introduction

Due to their inherent advantages in device design and also their simple integration in some complex systems, thin films semiconductor materials are preferred over their bulk counterparts [1–3]. The important class of semiconductor thin films are the films made from belong to II-VI compounds [4], due to a large-scale industrial applications, among of them ZnO. Recently, a lot of research efforts have been extensively studied the zinc oxide (ZnO) as form of thin films, since it has unique chemical and physical properties compared to other (Transparent Conductive Oxides) materials. Previous reported works examined structural, morphological, electrical, optical properties of ZnO thin films [5–10].

Zinc oxide (ZnO) is one of the most attractive transparent and conducting oxides (TCO) due to their wide direct band gap (3.3 eV) at room temperature [11], high electrochemical stability, abundance in nature, low toxicity [12], high exciton binding energy [13] and good electrical and optical properties. It is grown as n-type. Based on the mentioned advantages, it becomes one of the best candidates in many important applications in optoelectronics such as, transparent conductive electrodes, solar cells, and lasers [14,15].

Several techniques, like sol–gel process, Radio Frequency magnetron sputtering, pulsed laser deposition [16], chemical vapor deposition (CVD), electrochemical deposition [17], chemical bath deposition [18]

* Corresponding author.
E-mail address: ab_attaf@univ-biskra.dz (A. Attaf).

https://doi.org/10.1016/j.mseb.2021.115525
Received 16 April 2021; Received in revised form 5 September 2021; Accepted 7 November 2021
Available online 16 November 2021
0921-5107/© 2021 Elsevier B.V. All rights reserved.

and spray ultrasonic [19], were largely used to deposit ZnO thin films. Among of them, the ultrasonic spray technique is chosen herein as cost-effective and efficient method to deposit ZnO thin films since it is easy to control, allows obtaining uniform and high homogenous distribution even in large scale [20].Until now, there is no any researches on the studies that includes the influence of ultrasonic wave amplitude on ZnO thin film synthesized by ultrasonic spray technique. This motivates us to focus on this important factor and its influence on the physical properties of ZnO thin films.

The aim of the present work is to investigate and highlight the effect of the ultrasonic wave amplitude during the deposition of ZnO thin films. The structural, morphological, optical, and electrical properties of the deposited ZnO thin films were studied and reported in detail, indicating the crucial role of the ultrasonic wave amplitude to obtain a high quality Zinc oxide with better electrical and optical properties.

2. Experimental details

2.1. Materials and ZnO thin film preparation

The undoped films were deposited by the spray ultrasonic technique (see Fig. 1). The precursor salts, Zinc acetate dihydrate ($Zn(CH_3COO)_2{\cdot}2H_2O$) of 99.99% purity were used to synthesize ZnO thin films. The respective solutions were prepared for a concentration of 0.1 M by dissolving ($Zn(CH_3COO)_2{\cdot}2H_2O$) in 30 mL of methanol ($CH_3OH$).The solution was stirred thoroughly for two hours to obtain a complete homogeneity and transparent solution; then sprayed manually over the pre-heated glass substrates (micro-slides of dimensions 20 × 15 × 1.5 mm^3) kept at 400 °C. The atomizer feeding by a solution through a flow rate controller, and the incoming solution were atomized via ultrasonic wave delivered from a generator (Sonics vibra-cell model VCX 130 PB). We used the air as the carrier gas with pressure equal to 1.5 bar.

First of all, the substrates were cleaned several times successively with acetone, ethanol and double distilled water and subsequently dried in air. When the aerosol droplets arrive onto the heated substrate surface, the following chemical reaction occurs for formation highly adherent ZnO thin films:

$$\left(Zn(CH_3COO)_2.2H_2O\right)+CH_3OH+\frac{3}{2}O_2\rightarrow ZnO(s)+CO_2(g)+2CH_3COOH(g)+3H_2O(g)$$

The optimized experimental parameters used in our work are illustrated in Table 1. To study the ultrasonic wave amplitude effects on the physical properties of ZnO, we varied the amplitude percentage of the ultrasonic generator from 20% to 60%.

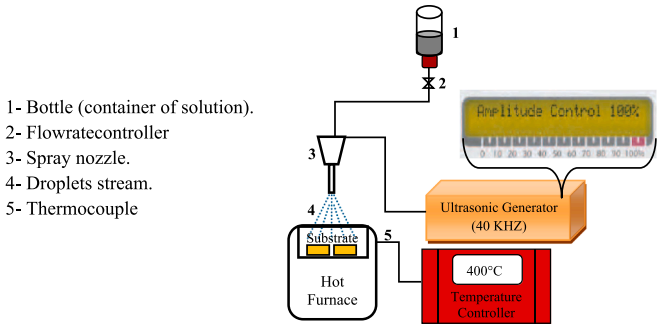

Fig. 1. Schematic diagram of the spray ultrasonic setup.

Table 1
Optimized spray parameters for ZnO thin films.

Experimental conditions	
Spray mode	Ultrasonic spray
Ultrasonic wave amplitude (%)	20, 30, 40, 50, and 60
Distance nozzle–substrate (mm)	40
Frequency of ultrasonic waves	40 KHZ
Concentration (mol/l)	0.1
Deposition temperature (°C)	400
Deposition time (min)	10
Carrier gas (air) pressure	1.5 bar

2.2. Characterization studies

The X-ray diffraction (XRD) patterns were recorded with a "Bruker D8"diffracto-meter with CuK_α radiation (θ–2θ scan) in the range of 20–55°.The surface morphology was examined using a scanning electron microscope "SEM JEOL model JSM 6301F", by which the film thickness was determined directly from the cross-sectional view by calculating the average thickness in all of the prepared samples. Besides, the optical characteristics of the ZnO films were measured using a UV–Vis spectrophotometer "model Perkin Elmer Lambda 1050" in the range from 200 nm to 2000 nm at room temperature. Finally, the electrical resistivity measurements were obtained using a" Jandel RM 3000" apparatus, by four-probe method, while Hall mobility and carrier concentration in the prepared films were measured by Hall effect measurements with applying the magnetic field 0.6 T and current 3 mA at room temperature.

3. Results and discussion

3.1. Thin film thickness

As well known, the growth of the films is one of the most important factor controlling the films properties. The dependency of the deposited films thickness with different ultrasonic wave amplitude is shown in Fig. 2. As seen, film thickness increases with increasing the ultrasonic

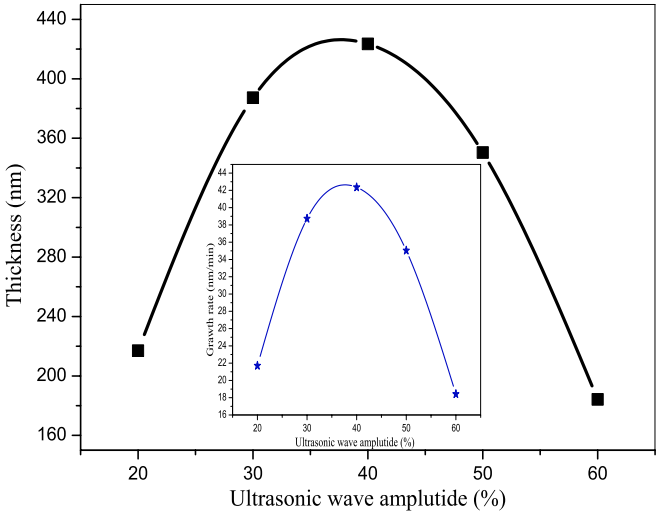

Fig. 2. Film thicknesses of ZnO thin films as a function of ultrasonic wave amplitude (inset of this figure the growth rate for ZnO thin films).

wave amplitude up to 40%, because low wave amplitude generates coarse droplets, which causes non-negligeable increases in mass transfer to the substrate and reaction kinetics, resulting in an augmentation in the growth rate of the films. An decrease in the films thickness was observed when the ultrasonic wave amplitude increases beyond 40%, this may be due to the diminished mass transport to the substrate surface due to gas convection and the increased rate of re-evaporation [21], resulted from the generated fine droplets at high wave amplitude. Similar behaviour of film thickness variation has been reported in early works [22,23].

3.2. Structural properties

The XRD patterns of the deposited thin films at various ultrasonic waves' amplitude are illustrated in Fig. 3. As can be seen, the obtained zinc oxide films are polycrystalline in nature. Two major peaks located at 2θ = 35.2° and 37.2° correspond respectively to (002) and (101) planes assigned to ZnO wurtzite hexagonal structure (JCPD: No. 36–1451), with a preferential orientation in the (002) direction indicating that the film growth is achieved along the c-axis, perpendicular to the substrate surface [24]. No other peaks correspond to secondary phases are detected, indicating the stoichiometry of the prepared ZnO samples. It is also worth noting that the (002) peak intensity is more pronounced and narrower due to the low formation energy required of this plane formation [25]. By the way, it is clear that the (002) intensity becomes more intense with increasing ultrasonic wave amplitude up to 40% and then decreases when the latter exceeds this percentage, while the (101) peaks begin to disappear with increasing ultrasonic wave amplitude. This indicates an improvement in the crystallinity for used ultrasonic wave amplitude less than 40%. Similar results were obtained by other literature [17,26] for ZnO thin films prepared using spray pyrolysis and spray ultrasonic technique at different spray flux density and substrate temperatures.

Moreover, we observed an apparent shift of (002) peak position towards smaller angles. The latter can be attributed to the occurrence of stress and defect during the growth film.

According to XRD patterns, the average crystallite size of the films was calculated using Debye Scherrer formula [27,28]:

$$D = \frac{0.94\lambda}{\beta\cos\theta} \quad (1)$$

where θ is the diffraction angle, λ is the XR wavelength (λ = 1.5418 Å), and β is the full width at half maxima (FWHM) in radians.

The defects in the ZnO films were estimated by calculating the dislocations density (δ) using Williamson relationship [29]:

$$\delta = \frac{1}{D^2} \quad (2)$$

The micro-strain (ξ) the ZnO films were calculated using the following equations [30]:

$$\xi = \frac{\beta}{4\tan(\theta)} \quad (3)$$

Table 2
Crystallite size, dislocation density and micro-strain of ZnO thin films extracted from XRD analysis.

UWA (%)	Peak (*hkl*)	2θ°	FWHM (β°)	D (nm)	Average D (nm)	δ (10^{14} lines/m^2)	ξ x10^{-4}
20%	(002)	35.31	0.36	24.2 ± 0.3	25.3	15.6	4.9
	(101)	37.04	0.33	26.5 ± 0.3			
30%	(002)	35.27	0.33	26.4 ± 0.3	26.9	13.8	4.6
	(101)	37.28	0.32	27.4 ± 0.3			
40%	(002)	35.21	0.28	31.1 ± 0.3	30	11.1	4.1
	(101)	37.04	0.30	29.2 ± 0.3			
50%	(002)	35.18	0.30	29 ± 0.3	25	16	5.1
	(101)	37.28	0.42	21 ± 0.3			
60%	(002)	35.12	0.38	23 ± 0.3	23	19	5.2

The variation of crystallite size, dislocation density and the micro-strain with ultrasonic wave amplitude of ZnO films are illustrated in Table 2 and Fig. 4.

According to Fig. 4; the crystallite size and micro-strain of the films have an opposite correlation. Further, it can be seen that the crystallite size increased from 25 to 30 nm for low ultrasonic wave amplitude (40%), and begins to decreases above 40%. Whereas, the micro-strain are well inverted to the crystallite size. Kim et al. [31] reported comparable results for Ni-doped ZnO and also Aida et al. [32] in Li-doped ZnO. Enhancement of crystallite size could be explained by augment the number of nucleation center and coalescence during film growth due to increase in both surface diffusivity and mobility of incoming sprayed particles at higher substrate temperature, thereby induces a better grain

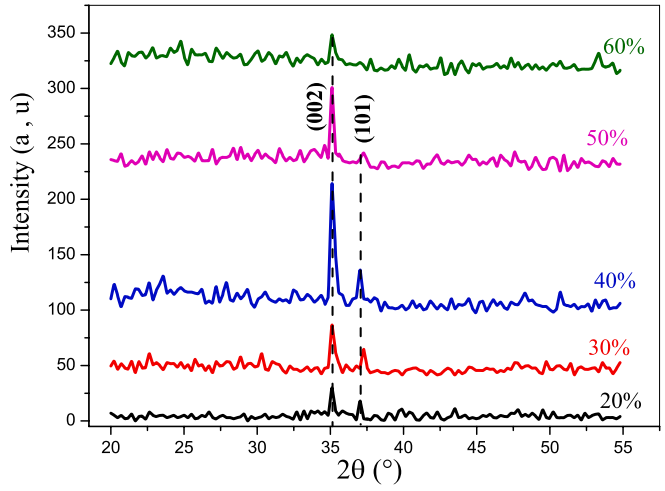

Fig. 3. X-ray diffraction patterns of ZnO films with different ultrasonic wave amplitude.

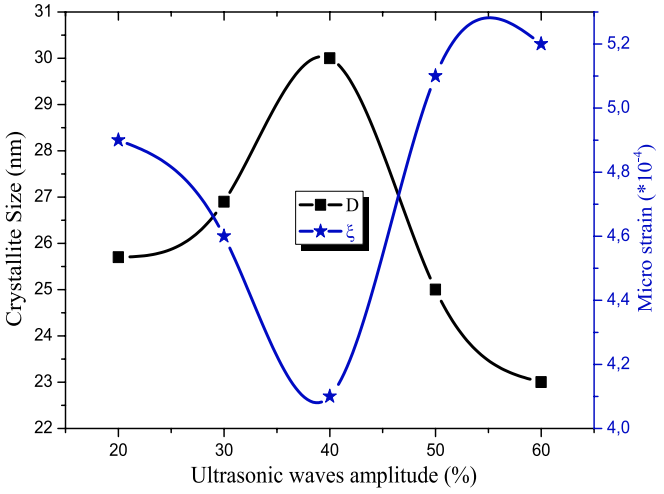

Fig. 4. Evolution of the crystallites size and micro-strain of the ZnO thin films at different ultrasonic wave amplitude.

coalescence and form clusters (nuclei) [33,34].

The decrement in the crystallite size from 30 to 23 nm at high ultrasonic wave amplitude can be attributed to increasing rate of re-evaporation resulting to decreases the small crystallites coalescence, hence the increased in total grains boundary, consequently the defects density increases [35].

From Bragg's law; the d-spacing for planes for h, k and l miller indices is given by equation [36]:

$$n\lambda = 2d_{hkl}\sin\theta_{hkl} \quad (4)$$

From the above equation n represents the diffraction order (n = 1)

The lattice constant c was determined for the ZnO hexagonal phase using the following relation-ship [37]:

$$\frac{1}{d^2} = \frac{4}{3}\left(\frac{h^2 + k^2 + hk}{a^2}\right) + \frac{l^2}{c^2} \quad (5)$$

Using the biaxial stress–strain model [38,39], we can calculate quantitatively the film stress (σ) and strain (ε) in the crystals with a highly c-axis preferred orientation. The film stress (σ) is parallel to the film surface and the strain (ε) in the films is along the c-axis, obtained by means of the following formulas:

$$\varepsilon = \frac{c_{film} - c_0}{c_0} \quad (6)$$

$$\sigma = \left(\frac{2c_{13}^2 - c_{33}(c_{11} + c_{12})}{2c_{13}}\right) \times \varepsilon = -233 \times \varepsilon\ (GPa) \quad (7)$$

where, $C_{11} = 208.8$ GPa, $C_{33} = 213.8$ GPa, $C_{12} = 119.7$ Gpa and $C_{13} = 104.2$ GPa for the stiffness constants of bulk ZnO, c_{film} represents the lattice constant of c-axis for the ZnO film calculated from X-ray diffraction data, and $c_0 = 5.206$ is the bulk lattice constant for ZnO powders.

The obtained structural parameters from XRD pattern and the internal stress in the prepared thin films are shown in Table 3.

One can deduce from the Table 3, a positive tensile stress in the pure ZnO film and this suggesting to that the lattice constant c is lower than the unstressed lattice parameter of bulk ZnO. Similar slightly smaller c values were also reported by Rahal et al. [40], and Islam et al. [41] for nano-crystalline Cd-doped ZnO and Al-doped ZnO thin films prepared by a sol–gel method.

The Fig. 5 shows the evolution of c(Å) and stress produced in thin layers, depending on the ultrasonic wave amplitude. Indeed, we noted that the parameters of lattice c(Å) increase with the increase of the ultrasonic wave amplitude, while the stress σ(GPa) decrease. The difference in c lattice parameter has to be attributed to the occurrence of stress in the obtained films. In general, the coefficient of thermal expansion (CTE) between the substrate material and the prepared thin film is suggested to induce a stress in the film [42]. The CTE of the glass [43] is

Table 3
Structural information obtained from XRD patterns and internal stress for ZnO thin films at different ultrasonic wave amplitude.

UWA (%)	h k l planes	2θ (°)	Calculated parameters		Reference parameter (JCPDS card No 36–1451)	Stress σ (GPa)
			Lattice constant c (Å)	d-spacing (Å)		
20	(002)	35.31	5.084 ± 0.01	2.542	$c_0 = 5.206$ Å d = 2.603 Å	5.5
30	(002)	35.27	5.090 ± 0.01	2.545		5.2
40	(002)	35.21	5.098 ± 0.01	2.549		4.8
50	(002)	35.18	5.102 ± 0.01	2.551		4.6
60	(002)	35.12	5.110 ± 0.01	2.555		4.3

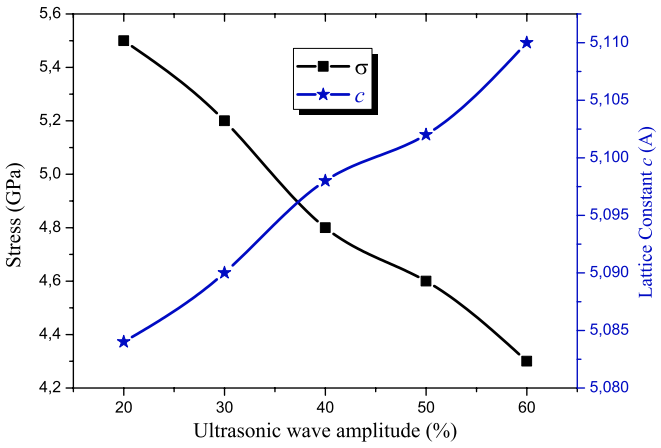

Fig. 5. The variation of the lattice parameters and c(Å) and the stress in the deposited ZnO thin films as function of ultrasonic wave amplitude.

3.17×10^{-6} K^{-1}, which is close to the CTE of ZnO (4.75×10^{-6} K^{-1}at 700 K) [44,45].

On the other hand, the stress in the film is associated with defects and impurities (imperfection), which in turn is related by density of the grain boundary. The grain boundary is one of the primary factors influencing the lattice defects. With the increase of ultrasonic wave amplitude the grain size increases which in turn decrease the number of grain boundary, resulting in decreased tensile stress [46,47].

3.3. Morphological properties

The dependency of surface characteristics in ZnO layers on ultrasonic wave amplitude was analysed by SEM, as Fig. 6(a)–(e) shows.

From the micrographs, one can see that the film shows better adherent to the substrate surface, and the surface is well covered. The micrograph clearly indicates that the surface morphology of all ZnO films is homogeneous, continuous and dense without any voids and cracks. In addition, all films exhibit granular appearance of uniform size distribution with regular more tightly packed nano-grains. Also, SEM images show that the morphology of the ZnO thin film has relatively smooth surface. The range of grain sizes from SEM image is found to be within 60–255 nm, depending on the ultrasonic wave amplitude value. The estimated grain size from the SEM micrographs is found to be obviously high than the crystallite size (see Table 2) that was calculated using the Scherrer formula, which could be owing to the agglomeration of small grains to form large crystallites [48,49]. Also, the SEM micrographs reveal that the average crystallite size increases up to 40%, then it decreases. This result is well agreement with the XRD results. In general, the cross sectional images showing that the films grow along the c axis with a good columnar structure (perpendicular shape).

3.4. Optical properties

The transmittance spectra of the films in the wavelength range of 200–2000 nm for the all samples are shown in Fig. 7. As we can see, the average transmittance of all films is greater than 80% in the visible region (400–800 nm). The same results have been reported in the literature [50,51].The highly transparent of the films is important for optical and optoelectronic applications, especially for solar cell window layers, and this suggests that these films have few internal defects and good crystallinity. In addition, the optical transmittance spectra of the most films have interference fringes in the visible region, which is due to the smooth surface of the films and the interference between the air-film and film-substrate interfaces [52,53]. Also, it can be seen from Fig. 7, a strong absorption in the ultraviolet region (λ less than 400 nm), which indicates that the films have a fundamental absorption owing to the

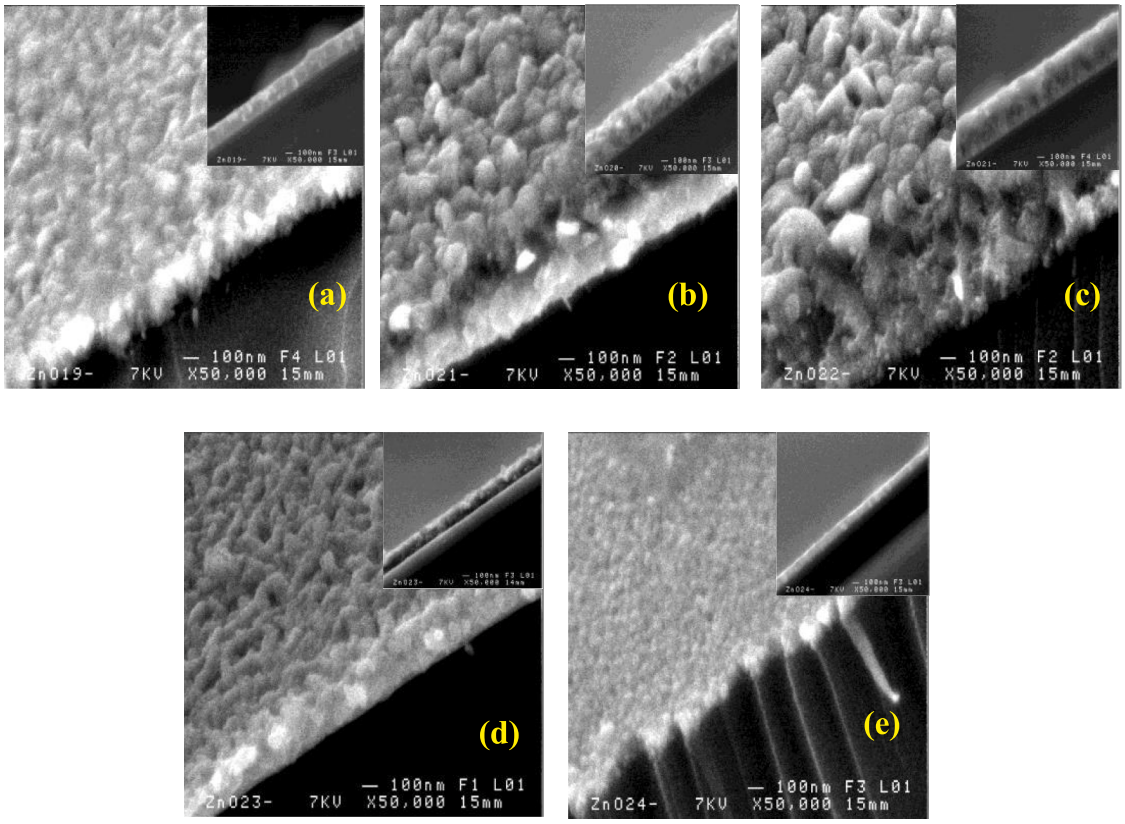

Fig. 6. SEM micrographs of ZnO films grown on glass substrate at different ultrasonic wave amplitude: (a) 20%, (b) 30%, (c) 40%, (d) 50% and (e) 60%.

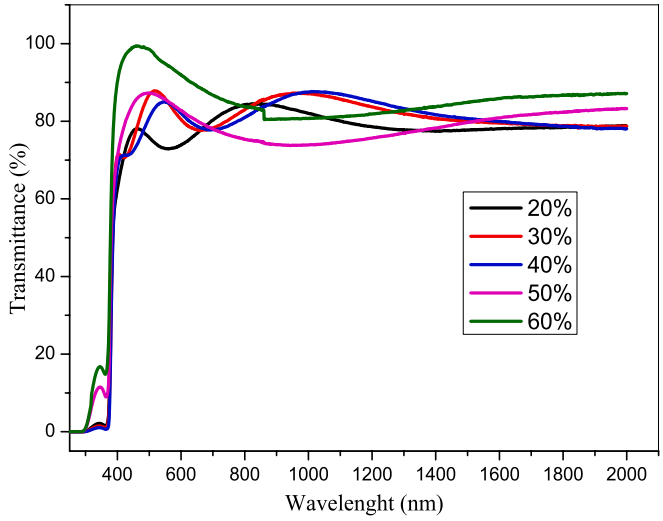

Fig. 7. Optical transmittance spectra of ZnO thin films prepared with different ultrasonic wave amplitude.

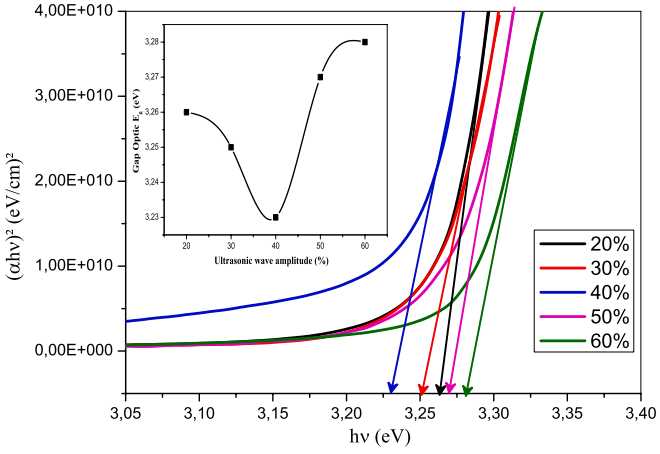

Fig. 8. Plots of$(\alpha h\nu)^2$ vs. (hν) for ZnO thin films. The inset shows variation of energy band gap as a function of ultrasonic wave amplitude.

electronic transition inter-band (the transition between the valence band and the conduction band).

The optical band gap energy of the prepared films has been determined from the transmittance spectra (the absorption edge) by applying the Tauc relation [54]:

$$(\alpha h\nu)^2 = A\left(h\nu - E_g\right) \tag{8}$$

where $h\nu$ is the photon energy, A is a constant, E_g is the optical band gap energy and α is the absorption coefficient, calculated as follow:

$$\alpha = \frac{1}{d} Ln\left(\frac{1}{T}\right) \tag{9}$$

where d is the thickness of the sample.

From the Tauc diagrams of the prepared ZnO thin films (presented in Fig. 8) and at the inflexion, the extrapolation of the linear part of the plot $(\alpha h\nu)^2$ versus hν leads to the gap energy value.

The Urbach energy (E_u) values were calculated using the following equations [55]:

$$\alpha = \alpha_0 . exp\left(\frac{h\nu}{E_u}\right) \text{ and } E_u = \left(\frac{d[\alpha h\nu]}{d[h\nu]}\right)^{-1} \tag{10}$$

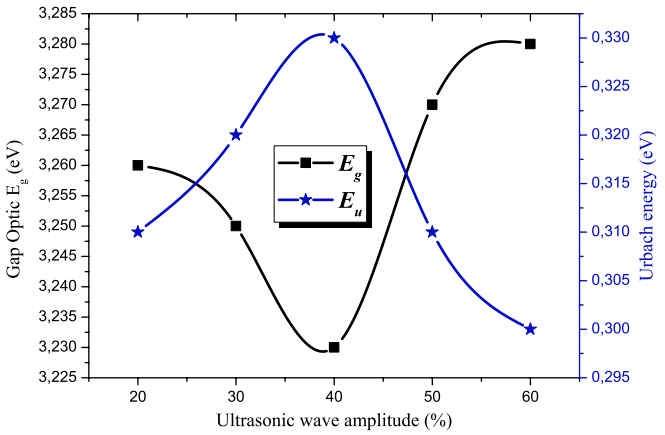

Fig. 9. The variation in the band gap energy and Urbach energy of ZnO films as a function of ultrasonic wave amplitude.

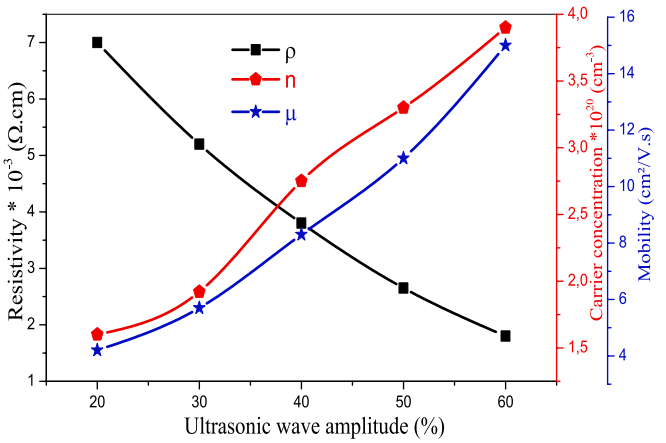

Fig. 10. Electrical resistivity, carrier concentration and carrier mobility as a function ultrasonic wave amplitude for ZnO thin films.

where α_0 is a constant and E_u is the Urbach energy or disorder energy.

The variations in the band gap and Urbach energy as a function of ultrasonic wave amplitude are shown in Fig. 9. As we can see, when the ultrasonic wave amplitude is increased further from 20% to 40%, the band gap energy gradually decreases from 3.26 to 3.23 eV and then increases from 3.23 to 3.28 eV above 40%. On contradict, the Urbach energy varied inversely with the band gap values of the films. These results are in good agreement with those published by other authors [56–58].The decreasing of band gap energy is mainly attributed to the crystallinity enhancement due to the quantum size effect [59]. Whereas the broadening of band gap energy might be due to an increase in carriers concentration, known as Burstein-Moss effect [60]. The Urbach energy reduction suggests the defects density and impurities lowering in the ZnO thin film network. While, the increase in Urbach energy is attributed to the presence of large number of defects originating the oxygen deficiency (vacancies) in ZnO thin films [61–64].

The refractive index is calculated by Ravindra equations [65]:

$$n = 4.08 - 0.62 \times E_g \quad (11)$$

The refractive index of the prepared zinc oxide thin films at various ultrasonic waves' amplitude is depicted in Table 4. There are some mechanisms which can effect the refractive index, such as: compressive or tensile stress, film thickness, grain size and the films disorder. As shown in Table 4, there is a correlation between the refractive index and films thicknesses. The refractive index variation is in good matched with the variation of the films thickness, which is very reasonable. A similar behavior was found by Sta et al. [66] for TiO_2 thin films with different numbers of layers. As shown in Table 4, the refractive index changes from 2.045 to 2.080 and found to be close to some experimental results reported by recent research [67–69].

3.5. Electrical properties

The electrical properties of the obtained ZnO thin films prepared at various ultrasonic wave amplitudes were studied. Fig. 10 shows the variations of electrical resistivity, carrier concentration and carrier mobility with ultrasonic wave amplitude variation from 20% to 60%. From Fig. 10, one can see clearly that the resistivity of the prepared films is around 10^{-3} Ω.cm and it decreases from 7×10^{-3} to 1.8×10^{-3} Ω.cm with the increased of ultrasonic wave amplitude increasing. Whereas, the carrier concentrations and carrier mobility of all samples tend to rise with ultrasonic wave amplitude increasing. In fact, the resistivity decrease, the carrier concentration and mobility enhancement can be related to the film crystallinity improvement in one hand and to inherent defects in ZnO such as Zn interstitials and oxygen vacancies on the other hand. This defect behave as a donor defect and consequently increase the free electrons concentration [70].The electrical properties in ZnO thin films prepared by means of some other different methods is presented in Table 5 for comparison.

Table 4
Refractive index of ZnO thin film at different ultrasonic wave amplitude calculated by Ravindra equation.

UWA (%)	Band gap Eg (eV)	Films Thickness (nm)	Refractive index n
20	3.26	217 ± 3	2.058
30	3.25	387 ± 3	2.065
40	3.23	423.5 ± 3	2.080
50	3.27	350 ± 3	2.052
60	3.28	184 ± 3	2.045

4. Conclusion

In summary, high transparent conducting ZnO thin films were deposited on glass substrates by means of spray ultrasonic technique. The effect of the ultrasonic wave amplitude on the optical, morphological, structural and electrical properties of the obtained thin films have been investigated. The XRD study reveals that ZnO thin films have the hexagonal wurtzite structure with strong (0 0 2) preferential orientation. The crystallite sizes were affected by ultrasonic wave amplitude and it was found to be ranged from 23 to 30 nm. Furthermore, the surface morphology images indicated the granular morphology with a homogeneous and smooth uniform surface of the films without any micro-cracks. The film thickness shows stronger dependence with ultrasonic wave amplitude, it was in the range of 184–423.5 nm. In addition, deposited ZnO thin films exhibit a high transmittance over 80% in the visible region with an apparent shift of the absorption edges towards lower wavelengths, resulting the increase in the optical band

Table 5
Electrical properties of ZnO thin films prepared by different method.

Material	Resistivity (Ω.cm)	Carrier Concentration (cm^{-3})	Carrier Mobility (cm^2/V.s)	Reference
In:ZnO (25–800 nm thickness)	2.05×10^{-3} to 5.44×10^{-4}	1.148×10^{20} to 3.357×10^{20}	26.53 to 33.93	[55]
Co-doped Al + In:ZnO (0.5–2%)	0.109 to 4.27 $\times 10^{2}$	4.01×10^{17} to 6.57×10^{18}	2.97 to 6.38	[71]
S:ZnO (0–10%)	4.55×10^{-3} to 1.25×10^{-3}	3×10^{20} to 4.4×10^{21}	0.023 to 0.073	[72]
ZnO (20–60% UWA)	7×10^{-3} to 1.8×10^{-3}	1.6×10^{20} to 3.9×10^{20}	4.2 to 15	This work

gap from 3.23 eV to 3.28 eV, due to the Moss–Burstein effect. Moreover, the electrical resistivity, carrier concentration and carrier mobility values were sensitive to the ultrasonic wave amplitude.

Finally, the obtained results prove that the improvement of the ZnO thin films quality can be controlled by ultrasonic wave amplitude for optoelectronic device applications such as solar cell, UV detectors and light emitting diodes.

Declaration of Competing Interest

The authors declare that they have no known competing financial interests or personal relationships that could have appeared to influence the work reported in this paper.

References

[1] Y. Li, Y.Q. Fu, S.D. Brodie, M. Alghane, A.J. Walton, Enhanced micro-droplet splitting, concentration, sensing and ejection by integrating ElectroWetting-On-Dielectrics and Surface Acoustic Wave technologies, in: 2011 16th International Solid-State Sensors, Actuators and Microsystems Conference, TRANSDUCERS'11, 2011, pp. 2936–2939.

[2] F. Bouhjar, L. Derbali, B. Marí, High performance novel flexible perovskite solar cell based on a low-cost-processed ZnO: Co electron transport layer, Nano Res. 13 (2020) 2546–2555.

[3] Feriel Bouhjar, Lotfi Derbali, Bernabé Marí, Brahim Bessaïs, Electrodeposited chromium-doped α-F_e2_O3 under various applied potential configurations for solar water splitting, Results Phys. 17 (2020), 102996.

[4] Tulay Hurma, Structural optical and electrical characterization of nanoparticle B doped ZnS films, Mater. Sci. -Poland 0072 (2019).

[5] A. Mosbah, S. Abed, N. Bouhssira, M.S. Aida, E. Tomasella, Preparation of highly textured surface ZnO thin films, Mater. Sci. Eng., B 129 (1-3) (2006) 144–149.

[6] A. Mosbah, A. Moustaghfir, S. Abed, N. Bouhssira, M.S. Aida, E. Tomasella, M. Jacquet, Comparison of the structural and optical properties of zinc oxide thin films deposited by d.c. and r.f. sputtering and spray pyrolysis, Surf. Coat. Technol. 200 (1-4) (2005) 293–296.

[7] N. Bouhssira, S. Abed, E. Tomasella, J. Cellier, A. Mosbah, M.S. Aida, M. Jacquet, Influence of annealing temperature on the properties of ZnO thin films deposited by thermal evaporation, Appl. Surf. Sci. 252 (15) (2006) 5594–5597.

[8] N. Lehraki, S. Abed, M.S. Aida, N. Attaf, A. Attaf, C. Poulain, ZnO thin films deposition by spray pyrolysis: influence of precursor solution, Curr. Appl Phys. 12 (2012) 1283.

[9] S. Benard, Mwankemwa, Shadrach Akinkuade, Kelebogile Maabong, Jackie M. Nel, Mmantsae Diale, Effect of surface morphology on the optical and electrical properties of schottky diodes of CBD deposited ZnO nanostructures, Phys. B: Condens. Matter 535 (2018) 175–180.

[10] M.I. Khan, K.A. Bhatti, L.G. RabiaQindeel, N.A. Bousiakou, Fazal-e-Aleem, Investigation of the structural, morphological and electrical properties of multilayer ZnO/TiO_2 thin films, deposited by sol-gel technique, Results Phys. 6 (2016) 156–160.

[11] Burak Kadem, Hikmat Adnan Banimuslem, Aseel Hassan, Modification of morphological and optical properties of ZnO thin film, Karbala Int. J. Mod. Sci. 3 (2) (2017) 103–110.

[12] M. Ajili, N. Jebbari, N. Kamoun Turki, M. Castagné, Effect of Al-doped on physical properties of ZnO Thin films grown by spray pyrolysis on SnO2: F/glass, in: EPJ Web of Conferences, 2012, p. 00002, https://doi.org/10.1051/epjconf/20122900002.

[13] Murat Tomakin, Zuhal Onuk, Nopporn Rujisamphan, Syed Ismat Shah, Role of the radio frequency magnetron sputtered seed layer properties on ultrasonic spray pyrolyzedZnO thin films, Thin Solid Films 642 (2017) 163–168.

[14] R. Parthiban, D. Balamurugan, B.G. Jeyaprakash, Spray deposited ZnO and Ga doped ZnO based DSSC with bromophenol blue dye as sensitizer: Efficiency analysis through DFT approach, Mater. Sci. Semicond. Process. 31 (2015) 471–477.

[15] Vinod Kumar, Fouran Singh, O.M. Ntwaeaborwa, H.C Swart, Effect of Br^{+6} ions on the structural, morphological and luminescent properties of ZnO/Si thin films, Appl. Surf. Sci. 279 (2013) 472–478.

[16] H. Ait Dads, S. Bouzit, L. Nkhaili, A. Elkissani, A. Outzourhit, Structural, optical and electrical properties of planar mixed perovskite halides/Al-doped Zinc oxide solar cells, Sol. Energy Mater. Sol. Cells 148 (2016) 30–33.

[17] U. Alver, T. Kılınc, E. Bacaksız, S. Nezir, Temperature dependence of ZnO rods produced by ultrasonic spray pyrolysis method, Mater. Chem. Phys. 106 (2007) 227–230.

[18] P. Hari, M. Baumer, W.D. Tennyson, L.A. Bumm, ZnOnanorods growth by chemical bath method, J. Non-Cryst. Solids 354 (2008) 2843–2848.

[19] H. Bendjedidi, A. Attaf, H. Saidi, M.S. Aida, S. Semmari, A. Bouhdjar, Y. Benkhetta, Properties of n-type SnO_2 semiconductor prepared by spray ultrasonic technique for photovoltaic applications, J. Semicond. 36 (12) (2015), 123002(1-4).

[20] R. Mimouni, N. Mahdhi, K. Boubaker, A. Madouri, M. Amlouk, Physical study on Cobalt-Indium Co-doped ZnOnanofilms as hydrophobic surfaces, Superlattices Microstruct. 91 (2016) 345–357.

[21] Ki Hyun Yoon, Joon Yeob Cho, Photoluminescence characteristics of zinc oxide thin films prepared by spray pyrolysis technique, Mater. Res. Bull. 35 (1) (2000) 39–46.

[22] Mohamed Othmane, Abdallah Attaf, Hanane Saidi, Fouad Bouaichi, Nadia Lehraki, Malika Nouadji, Marcel Poulain, Said Benramache, Modulation of physical properties of sprayed ZnO thin films by substrate temperature for optical applications, Int. J. Nanosci. 15 (1 & 2) (2016), 1650007 (8 pages).

[23] Fouad Bouaichi, Hanane Saidi, Abdallah Attaf, Mohamed Othmane, Nadia Lehraki, Malika Nouadji, Marcel Poulain, Said Benramache, The synthesis and characterization of sprayed ZnO thin films: as a function of solution molarity, Main Group Chem. 15 (2016) 57–66.

[24] H. Belkhalfa, H. Ayed, A. Hafdallahd, M.S. Aida, R. TalaIghil, Characterization and studying of ZnO thin films deposited by spraypyrolysis: effect of annealing temperature, Optik 127 (2016) 2336–2340.

[25] Saad Rahmane, Mohamed Abdou Djouadi, Mohamed Salah Aida, Nicolas Barreau, Oxygen effect in radio frequency magnetron sputtered aluminium doped zinc oxide films, Thin Solid Films 562 (2014) 70–74.

[26] R. Mohan, K. Ravichandran, A. Nithya, K. Jothivenkatachalam, C. Ravidhas, B. Sakthivel, Influence of spray flux density on the photocatalytic activity and certain physical properties of ZnO thin films, J. Mater. Sci.: Mater. Electron. 25 (6) (2014) 2546–2553.

[27] Z. Qiao, R. Latz, D. Mergl, Thickness dependence of In_2O_3: Sn film gowth, Thin Solid Films 466 (2004) 250.

[28] M.M. Bagheri-Mohagheghi, N. Shahtahmasebi, M.R. Alinejad, A. Youssefi, M. Shokooh-Saremi, The effect of the post-annealing temperature on the nano-structure and energy band gap of SnO_2 semiconducting oxide nanoparticles synthesized by polymerizing-complexing sol-gel method, Phys. B Condens. Matter 403 (2008) 2431–2437.

[29] I. Bouhaf Kherkhachi, A. Attaf, H. Saidi, A. Bouhdjar, H. Bendjdidi, Y. Benkhetta, R. Azizi, M.S. Aida, Structural, morphological, optical and electrical characterization of spray ultrasonic deposited SnS2thin film, Optik 127 (2016) 2266–2270.

[30] C. Mrabet, O. Kamoun, A. Boukhachem, M. Amlouk, T. Manoubi, Some physical investigations on hexagonal-shaped nanorods of lanthanum-doped ZnO, J. Alloys Compd. 648 (2015) 826–837.

[31] K. Kim, G. Kim, J. Woo, C. Kim, Characteristics of Nickel-doped Zinc Oxidethin films prepared by sol–gel method, Surf. Coat. Technol. 202 (22-23) (2008) 5650–5653.

[32] M.S. Aida, M. Hjiri, Temperature dependent photoluminescence of Li-doped ZnO, J. Mater. Sci.: Mater. Electron. 31 (13) (2020) 10521–10530.

[33] A. Sanchez-Juarez, A. Tiburcio-Silver, A. Ortiz, Properties of fluorine-doped ZnO deposited onto glass by spray pyrolysis, Sol. Energy Mater. Sol. Cells 52 (1998) 301–311.

[34] P. Chelvanathan, Y. Yusoff, F. Haque, M. Akhtaruzzaman, M.M. Alam, Z. A. Alothman, M.J. Rashid, K. Sopian, N. Amin, Growth and characterization of RF-sputtered ZnS thin film deposited at various substrate temperatures for photovoltaic application, Appl. Surf. Sci. 334 (2015) 138–144.

[35] A. Derbali, H. Saidi, A. Attaf, H. Benamra, A. Bouhdjer, N. Attaf, H. Ezzaouia, L. Derbali, M.S. Aida, Solution flow rate influence on ZnS thin films properties grown by ultrasonic spray for optoelectronic application, J. Semicond. 39 (9) (2018), 093001-(1 to 7).

[36] Kamal A. Aly, N.M. Khalil, Yousif Algamal, Qaid M.A. Saleem, Estimation of lattice strain for zirconia nano-particles based on Williamson- Hall analysis, Mater. Chem. Phys. 193 (2017) 182–188.

[37] Imen Bouhaf Kherchachi, Hanane Saidi, Abdallah Attafa, Nadir Attaf, Adel Bouhdjar, Hamzabendjdidi, Youcef Benkhetta, Rahil Azizi, Mohamed Jlassi, Influence of solution flow rate on the properties of SnS2filmsprepared by ultrasonic spray, Optik 127 (2016) 4043–4046.

[38] R. Hong, J. Shao, H. He, Z. Fan, Influence of buffer layer thickness on the structure and optical properties of ZnO thin films, Appl. Surf. Sci. 252 (2006) 2888–2893.

[39] Shaban, A. El Sayed, Effects of lanthanum and sodium on the structural, optical and hydrophilic properties of sol–gel derived ZnO films: a comparative study, Mater. Sci. Semicond. Process. 41 (2016) 323–334.

[40] Badis Rahal, Boubekeur Boudine, Youssef Larbah, Lakhdar Guerbous, Miloud Sebais, Ouahiba Halimi, Menouar Siad, Sol-gel synthesis and nano-structured semiconductor analysis of undoped and Cd-doped ZnO thin films, Optik 169 (2018) 303–313.

[41] Muhammad R. Islam, S.F.U. MukhlasurRahman, J. Podder Farhad, Structural, optical and photocatalysis properties of sol–gel deposited AldopedZnO thin films, Surf. Interfaces 16 (2019) 120–126.

[42] Fang-Hsing Wang, Chiao-Lu Chang, Effect of substrate temperature on transparent conducting Al and Fco-doped ZnO thin films prepared by rf magnetron sputtering, Appl. Surf. Sci. 370 (2016) 83–91.

[43] C.F. Klingshirn, B.K. Meyer, A. Waag, A. Hoffmann, J. Geurts, in: Zinc Oxide: from Fundamental Properties towards Novel Applications, Springer-Verlag, Berlin Heidelberg, 2010, p. 11.

[44] H. Belkhalfa, H. Ayed, A. Hafdallahd, M.S. Aidad, R. TalaIghil, Characterization and studying of ZnO thin films deposited by spray pyrolysis: effect of annealing temperature, Optik 127 (2016) 2336–2340.

[45] W. Water, S.Y. Chu, Physical and structural properties of ZnO sputtered films, Mater. Lett. 55 (2002) 67–72.

[46] T. Prasada Rao, M.C. Santhosh Kumar, V. Ganesan, M.C. Santhosh Kumar, V. Ganesan, Effect of annealing on the structural, optical and electrical properties of ZnO thin films by spray pyrolysis, India J. Phys 85 (9) (2011) 1381–1391.

[47] G.G. Rusu, A.P. Rambu, V.E. Buta, M. Dobromir, D. Luca, M. Rusu, structural and optical characterization of Al-doped ZnO films prepared by thermal oxidation of evaporated Zn/Al multilayered films, Mater. Chem. Phys. 123 (2010) 314–321.
[48] A. Rmili, F. Ouachtari, A. Bouaoud, A. Louardi, T. Chtouki, B. Elidrissi, H. Erguig, Structural, optical and electrical properties of Ni-doped CdS thin films prepared by spray pyrolysis, J. Alloys Compd. 557 (2013) 53–59.
[49] H. Benamra, H. Saidi, A. Attaf, M.S. Aida, A. Derbali, N. Attaf, Physical properties of Al-doped ZnS thin films prepared by ultrasonic spray technique, Surf. Interfaces 21 (2020), 100645.
[50] Said Benramache, Boubaker Benhaoua, Foued Chabane, Abderrazak Guettaf, A comparative study on the nanocrystalline ZnO thin films prepared by ultrasonic spray and sol–gel method, Optik 124 (2013) 3221–3224.
[51] Vinoth Kumar Jayaraman, Arturo Maldonado Álvarez, , Effect of precursor type and doping concentration on the physical properties of ultrasonically sprayed aluminium and indium co-doped zinc oxide thin films, Thin Solid Films 642 (2017) 14–19.
[52] A. Yahia, A. Attaf, H. Saidi, M. Dahnoun, C. Khelifi, A. Bouhdjar, A. Saadi, H. Ezzaouia, Structural, optical, morphological and electrical properties of indium oxide thin films prepared by sol gel spin coating process, Surf. Interfaces 14 (2019) 158–165.
[53] Ahmed R. Hegazy, B. Salameh, A.M. Alsmadi, Optical transitions and photoluminescence of fluorine-doped zinc tin oxide thin films prepared by ultrasonic spray pyrolysis, Ceram. Int. 45 (2019) 19473–19480.
[54] A. Attaf, A. Derbali, H. Saidi, H. Benamra, M.S. Aida, N. Attaf, H. Ezzaouia, L. Derbali, Physical properties of Pb doped ZnS thin films prepared by ultrasonic spray technique, Phys. Lett. A 384 (2020), 126199.
[55] Du-Cheng Tsai, Zue-Chin Chang, Bing-Hau Kuo, Yu-Hong Wang, Erh-Chiang Chen, Fuh-Sheng Shieu, Thickness dependence of the structural, electrical, and optical properties of amorphous indium zinc oxide thin films, J. Alloys Compd. 743 (2018) 603–609.
[56] A. Rahal, S. Benramache, B. Benhaoua, Substrate temperature effect on optical property of ZnOThin films, Eng. J. Canada 18 (2) (2014) 81–88.
[57] I.Y. Erdogan, The alloying effect on the structural and optical properties of nanocrystalline copper zinc oxide thin films fabricated by spin coating and annealing method, J. Alloys Compd. 502 (2010) 445–450.
[58] A.H. Mehnaz, Sharmin Bhuiyan, Influence of substrate temperature on the properties of spray deposited nanofibrous zinc oxide thin films, Appl. Phys. A 124 (2018) 57.
[59] A. Derbali, A. Attafa, H. Saidi, H. Benamra, M. Nouadji, M.S. Aida, N. Attaf, H. Ezzaouia, Investigation of structural, optical and electrical properties of ZnS thin films prepared by ultrasonic spray technique for photovoltaic applications, Optik 154 (2018) 286–293.
[60] A.R. Babar, S.S. Shinde, A.V. Moholkar, C.H. Bhosale, J.H. Kim, K.Y. Rajpure, Structural and optoelectronic properties of antimony incorporated tin oxide thin films, J. Alloys Compd. 505 (2010) 416–422.
[61] Y. Li, J. Gong, M.M. Cune, et al., I-V characteristics of the p–n junction between vertically aligned ZnOnanorods and polyaniline thin film, Synth. Met. 160 (2010) 499–503.
[62] R. Mimouni, K. Boubaker, M. Amlouk, Investigation of structural and optical properties in Cobalt-Chromium co-doped ZnO thin films within the Lattice Compatibility Theory scope, J. Alloys Compd. 624 (2015) 189–194.
[63] N. Chahmat, T. Souier, A. Mokri, M. Bououdina, M.S. Aida, M. Ghers, Structure, microstructure and optical properties of Sn-doped ZnO thin films, J. Alloys Compd. 593 (2014) 148–153.
[64] R. Ayouchi, F. Martin, D. Leinen, J.R. Ramos-Barrado, Growth of pure ZnO thin films prepared by chemical spray pyrolysis on silicon, J. Cryst. Growth 247 (3-4) (2003) 497–504.
[65] N.M. Ravindra, Preethi Ganapathy, Jinsoo Choi, Energy gap-refractive index relation in semiconductors– an overview, Infrared Phys. Technol. 50 (2007) 21–29.
[66] I. Sta, M. Jlassi, M. Hajji, M.F. Boujmil, R. Jerbi, M. Kandyla, M. Kompitsas, H. Ezzaouia, Structural and optical properties of TiO_2 thin films prepared by spin coating, J. Sol-Gel Sci. Technol. 72 (2) (2014) 421–427.
[67] H.A. Mohamed, Some physical properties of ZnO thin films prepared by thermal oxidation of metallic Zn, Optoelectron. Adv. Mater. 6 (3–4) (2012) 389–393.
[68] M. Mazilu, N. Tigau, V. Musat, Optical properties of undoped and Al-doped ZnO nanostructures grown from aqueous solution on glass substrate, Optik. Mater. 34 (11) (2012) 1833–1838.
[69] Younghun Hwang, Heejin Ahn, Manil Kang, Youngho Uma, Hyoyeol Park, Electronic and optical properties in ZnO:Ga thin films induced by substratestress, J. Phys. Chem. Solids 87 (2015) 122–127.
[70] Tianlei Ma, Effect of precursor concentration and sintering on functional properties of ZnO thin films deposited by aerosol-assisted chemical vapour deposition (AACVD), Mater. Sci. Semicond. Process. 121 (2021), 105413.
[71] Devika Mahesh, M.C. Santhosh Kumar, Synergetic effects of aluminium and indium dopants in the physical properties of ZnO thin films via spray pyrolysis, Superlattices Microstruct. 142 (2020), 106511.
[72] M.H. Haja sheriff, S. Murugan, A. Manivasaham, R. Ashok Kumar, Electro spray technique to enhance the physical property of sulphur doped zinc oxide thin film, Mater. Today:. Proc. 47 (2021) 1717–1723.